Spatiotemporal dynamics of charged species in the afterglow of plasmas containing negative ions

I. D. Kaganovich,* B. N. Ramamurthi, and Demetre J. Economou†
Plasma Processing Laboratory, Department of Chemical Engineering, University of Houston, 4800 Calhoun Road, Houston, Texas 77204-4004

(Received 18 April 2000; revised manuscript received 17 April 2001; published 27 August 2001)

The spatiotemporal evolution of charged species densities and wall fluxes during the afterglow of an electronegative discharge has been investigated. The decay of a plasma with negative ions consists of two stages. During the first stage of the afterglow, electrons dominate plasma diffusion and negative ions are trapped inside the vessel by the static electric field; the flux of negative ions to the walls is nearly zero. During this stage, the electron escape frequency increases considerably in the presence of negative ions, and can eventually approach free electron diffusion. During the second stage of the afterglow, electrons have disappeared, and positive and negative ions diffuse to the walls with the ion-ion ambipolar diffusion coefficient. Theories for plasma decay have been developed for equal and strongly different ion (T_i) and electron (T_e) temperatures. In the case $T_i = T_e$, the species spatial profiles are similar and an analytic solution exists. When detachment is important in the afterglow (weakly electronegative gases, e.g., oxygen) the plasma decay crucially depends on the product of negative ion detachment frequency (γ_d) and diffusion time (τ_d). If $\gamma_d \tau_d > 2$, negative ions convert to electrons during their diffusion towards the walls. The presence of detached electrons results in ''self-trapping'' of the negative ions, due to emerging electric fields, and the negative ion flux to the walls is extremely small. In the case $T_i \ll T_e$, the spatiotemporal dynamics is more complicated due to the presence of negative ion density fronts. During the afterglow, although negative ions diffuse freely in the plasma core, the negative ion fronts propagate towards the chamber walls with a nearly constant velocity. The evolution of ion fronts in the afterglow of electronegative plasmas is important, since it determines the time needed for negative ions to reach the wall, and thus influence surface reactions in plasma processing.

DOI: 10.1103/PhysRevE.64.036402 PACS number(s): 52.55.Dy

I. INTRODUCTION

Negative-ion-rich (electronegative) plasmas are of great importance in semiconductor manufacturing [1,2], negative ion sources [3,4], and the *D* layer of the lower ionosphere [5]. There often appear new and interesting phenomena in plasmas containing negative ions in addition to electrons and positive ions, see, for example, [6–8].

Pulsed plasmas (in which the power is turned on and off with a predetermined period and duty cycle) in electronegative gases have been shown to offer important advantages compared to their continuous wave (cw) counterparts. Properties of deposited films can be altered [9], and etch and deposition rate can be maintained despite the lower average power [10]. Recently, it has been recognized that pulsed plasmas may also ameliorate anomalous etch profiles (e.g., notching) and other forms of charging damage that occur in conventional continuous wave discharges [1,2]. The ratio of chemical species present in the plasma can be varied, e.g., production of negative ions can be increased in pulsed negative ion sources compared to conventional continuous discharges [3].

Negative ions are difficult to extract from cw plasmas because of the electrostatic fields due to the presence of electrons. When power is turned off in the afterglow, however, electrons disappear by diffusion to the walls and attachment to gas molecules. After some time in the afterglow, the electron density and temperature are too low for any significant electrostatic fields to exist, and a transition occurs from an electron-dominated plasma to a positive ion–negative ion (ion-ion) plasma [11–13]. After that time, it is possible to extract negative ions out of the plasma. Nevertheless, there can be situations for which the electron density in the afterglow does not decay to a level for the fields to completely disintegrate. An example is detachment of negative ions in the afterglow that generates new electrons. Under such circumstances it is possible for negative ions to remain trapped even in the late afterglow.

Another interesting phenomenon observed in pulsed plasmas of electronegative gases is the formation of negative ion density fronts, i.e., negative ion density profiles with very sharp gradients. During plasma ignition (power on), self-sharpening negative ion density fronts develop and move towards the plasma center [11], in analogy with hydrodynamic shocks. During the afterglow, negative ion fronts exist when $T_e \gg T_i$, and move towards the chamber walls. However, the latter fronts are of a different nature and have no direct analogy with hydrodynamic shocks. As it turns out, the negative ion front propagation speed is nearly constant (for constant electron and ion temperatures in the afterglow).

In this paper, we focus on physical phenomena associated with plasma diffusion to the containing vessel wall during the afterglow. The goal is to determine the spatiotemporal behavior of charged species profiles, to investigate the transition from electron-dominated plasma to ion-ion (electron-free) plasma, and to give analytic estimates of the transition time, needed for negative ions to reach the wall. Predicting

*Present address: Plasma Physics Laboratory, Princeton University, Princeton, NJ 08543. Email address: ikaganov@pppl.gov
†Email address: economou@uh.edu

this time is of importance for plasma applications that utilize negative ions extracted from the plasma.

The article is organized as follows: Sec. II contains the description of the model, Sec. III embodies analytical solutions for equal ion and electron temperatures ($T_i = T_e$) and comparison with laboratory experiments, and Sec. VIII is devoted to the case of $T_e \gg T_i$.

II. DESCRIPTION OF THE MODEL

We assume that the ion mean free path is smaller than the characteristic length scale and examine one-dimensional species transport in a parallel plate geometry. For a collisional plasma, the species fluxes are described by a drift-diffusion equation, $\Gamma_k = -D_k \partial n_k/\partial x \pm \mu_k n_k E$, where D_k and μ_k are the k-species diffusion coefficient and mobility, respectively, tied by the Einstein relation $D_k = T_k \mu_k$. T_k is the k-species temperature, in volts. The self-consistent electrostatic field can be found from the condition of zero net current $j = e(\Gamma_p - \Gamma_n - \Gamma_e) = 0$ and is given by

$$E = \frac{D_p \nabla p - D_n \nabla n - D_e \nabla n_e}{\mu_p p + \mu_n n + \mu_e n_e}. \quad (1)$$

Here, p, n, and e (also as subscripts) correspond to positive ions, negative ions, and electrons, respectively. If the electron density ($\mu_e n_e \gg \mu_n n, \mu_p p$) and its gradient are not too small, electrons are described by Boltzmann equilibrium: $E = -T_e/\nabla(\ln n_e)$.

Equation (1) for the electric field along with the mass continuity equations for negative ions and electrons and the electroneutrality constraint yield a system of equations that describes the spatiotemporal evolution of charged species densities, fluxes, and electric field.

$$\frac{\partial n}{\partial t} - \mu_n \frac{\partial}{\partial x}\left(T_i \frac{\partial n}{\partial x} + En \right) = \nu_{\rm att} n_e - \gamma_d n - \beta_{\rm ii} np, \quad (2a)$$

$$\frac{\partial n_e}{\partial t} - \mu_e \frac{\partial}{\partial x}\left(T_e \frac{\partial n_e}{\partial x} + En_e \right) = (Z_{\rm ioniz} - \nu_{\rm att}) n_e + \gamma_d n, \quad (2b)$$

$$n_e = p - n. \quad (2c)$$

In Eqs. (2), $\beta_{\rm ii}$ is the ion-ion recombination rate coefficient, and $Z_{\rm ioniz}$, $\nu_{\rm att}$, and γ_d are the ionization, attachment, and detachment frequencies, respectively.

In the afterglow, the electron temperature decreases drastically within a few microseconds, so that ionization switches off. If there is residual power coupled to the plasma during the afterglow, the electron temperature will reach a steady value such that $T_e \gg T_i$. Otherwise, the electron temperature will decay to essentially the gas temperature so that $T_e = T_i$. In either case, we assume that the electron temperature is a given constant in order to be able to derive analytic solutions.

Substituting the expression for electric field, Eq. (1), into the continuity equations for negative ions and electrons and using the electroneutrality constraint yields a new system of equations:

$$\frac{\partial n}{\partial t} - \frac{\partial}{\partial x}\left(\mu_i T_i \frac{\partial n}{\partial x} - un \right) = \nu_{\rm att} n_e - \gamma_d n - \beta_{\rm ii} np, \quad (3a)$$

$$\frac{\partial n_e}{\partial t} - \frac{\partial}{\partial x}\left[D_{\rm eff} \frac{\partial n_e}{\partial x} \right] = (Z_{\rm ioniz} - \nu_{\rm att}) n_e + \gamma_d n, \quad (3b)$$

$$n_e = p - n, \quad (3c)$$

$$u \equiv \frac{\mu_i T_e}{n_e + \mu_i/\mu_e (p+n)} \frac{\partial n_e}{\partial x}, \quad (3d)$$

$$D_{\rm eff} = \frac{\mu_i T_e (p+n)}{n_e + \mu_i/\mu_e (p+n)} + \mu_i T_i. \quad (3e)$$

For simplicity we have considered the case of equal ion mobilities and diffusion coefficients $\mu_p = \mu_n \equiv \mu_i$, $D_p = D_n \equiv D_i \equiv \mu_i T_i$. The system of Eqs. (3) is more transparent than the initial system of Eqs. (2), since Eq. (3b) is a purely diffusion-type equation, in contrast to the diffusion-drift-type Eq. (2b). In an electron-dominated plasma, $n_e \mu_e \gg \mu_i (p+n)$, the effective [Eq. (3e)] diffusion coefficient $D_{\rm eff} = \mu_i T_e (p+n)/n_e + \mu_i T_i$, of the order of the ambipolar diffusion coefficient, $\mu_i (T_i + T_e)$. In an ion-ion plasma, $n_e \mu_e \ll \mu_i (p+n)$, $D_{\rm eff} = \mu_e T_e$, the free electron diffusion coefficient. The ratio between the two $D_{\rm eff}$ can be of the order of 100, since the ratio of mobilities μ_e/μ_i is typically of the order of 100.

Boundary conditions for Eqs. (3a) and (3b) were: symmetry at the plasma center, and zero negative ion and electron densities (in reality, a very small value for density) at the wall. If the flux of negative ions at the wall was into the plasma, that flux was set equal to zero. This peculiar boundary condition corresponds to the absence of negative ion generation at the wall.

An implicit finite difference scheme was used to solve Eq. (3b), and an explicit scheme was used for Eq. (3a), because larger time steps are allowed for the latter equation. Typical execution times were a few minutes on a Pentium II PC.

III. AFTERGLOW WITH EQUAL ION AND ELECTRON TEMPERATURES ($T_i = T_e$), AND WITH DIFFUSION DOMINATING PARTICLE LOSS

In this section we provide a theoretical description of the spatiotemporal behavior of charged particle profiles, investigate the transition from electron-dominated plasma to ion-ion (electron-free) plasma, and give analytic estimates of the transition time. For a product of gas pressure and half-gap length, PL, higher than about 10 mTorr cm, the electron temperature decays much faster than the ion and electron densities [1,11,13]. We therefore investigate the afterglow evolution assuming equal ion and electron temperatures, $T_i = T_e \equiv T$.

The initial spatial profiles of ion and electron densities corresponding to an active discharge are very inhomogeneous [14] and are determined by the interplay of several system frequencies: $\nu_{\rm att}, \gamma_d, \beta_{\rm ii} p, D_i/\Lambda^2, D_{\rm eff}/\Lambda^2$, where $1/\Lambda = \pi/2L$ or $2.4/R$ is an effective diffusion length for slab

TABLE I. Frequency of diffusive loss of positive ions, negative ions, and electrons for $T_e = T_i$.

$F \equiv \frac{\mu_i(p+n)}{\mu_e n_e}$	Electron-dominated plasma ($F \ll 1$)	Ion-ion plasma ($F \gg 1$)	
$Z_{p,\mathrm{loss}} = \frac{D_i}{\Lambda^2}\left(1+\frac{1}{1+F}\right)$	$\frac{2D_i}{\Lambda^2}$	$\frac{D_i}{\Lambda^2}$	(6a)
$Z_{n,\mathrm{loss}} = \frac{D_i}{\Lambda^2}\left(\frac{F}{1+F}\right)$	$\frac{FD_i}{\Lambda^2}$	$\frac{D_i}{\Lambda^2}$	(6b)
$Z_{e,\mathrm{loss}} = \frac{D_i}{\Lambda^2}\left(1+\frac{p+n}{n_e(1+F)}\right)$	$\frac{2p}{n_e}\frac{D_i}{\Lambda^2}$	$\frac{D_e}{\Lambda^2}$	(6c)

or cylindrical geometry, respectively [15]. When plasma chemical processes are faster than diffusion losses, $\nu_{\mathrm{att}}, \gamma_d, \beta_{\mathrm{ii}} p \gg D_i/\Lambda^2, D_{\mathrm{eff}}/\Lambda^2$, the dynamic behavior is governed entirely by plasma chemical reactions. We shall consider mostly the opposite case when $\nu_{\mathrm{att}}, \gamma_d, \beta_{\mathrm{ii}} p < D_i/\Lambda^2, D_{\mathrm{eff}}/\Lambda^2$. After a short period in the afterglow all three density profiles are similar [16] (for a review see [15]),

$$\frac{n}{n_0} = \frac{p}{p_0} = \frac{n_e}{n_{e0}} = f\left(\frac{x}{\Lambda}\right), \tag{4}$$

where $f(x/\Lambda) = \cos(x/\Lambda)$ for slab geometry and $f(r/\Lambda) = J_0(r/\Lambda)$ for cylindrical geometry, J_0 is a Bessel function, and subscript zero in Eq. (4) signifies the central densities. Note that for unequal temperatures, the plasma profiles are not similar. Indeed, the assumption of similar profiles for $T_e > T_i$ results in a flux of negative ions directed from the wall into the plasma and, consequently, an artificial production of negative ions at the wall [16].

Similarity in the spatial profiles simplifies the problem considerably. For example, the spatiotemporal species density dynamics can be described by only the central values $p_0(t), n_0(t), n_{e0}(t)$. Also, the density ratios (e.g., p/n_e) are independent of position in view of Eq. (4). Substituting the value of electric field Eq. (1) into the expression for fluxes, one can find [17]

$$\Gamma_p(x,t) = \frac{D_i p_0}{\Lambda}\left(1+\frac{1}{1+F}\right) f'\left(\frac{x}{\Lambda}\right), \tag{5a}$$

$$\Gamma_n(x,t) = \frac{D_i n_e}{\Lambda}\frac{F}{1+F} f'\left(\frac{x}{\Lambda}\right), \tag{5b}$$

$$\Gamma_e(x,t) = \frac{D_i n_{e0}}{\Lambda}\left(1+\frac{p+n_e}{n_e(1+F)}\right) f'\left(\frac{x}{\Lambda}\right), \tag{5c}$$

with $F \equiv \mu_i(p+n)/(\mu_e n_e)$ and f' is the derivative of f. The frequency $Z_{k,\mathrm{loss}} \equiv \partial \ln n_k/\partial t$ of k-species diffusive loss can be found from Eqs. (5), and are shown in Table I.

From Eq. (5a) one can see that if $F \ll 1$, the effective diffusion coefficient of positive ions is $2D_i$. This result coincides with the ambipolar diffusion coefficient in isothermal electropositive plasmas composed of only electrons and positive ions. Note that this result is valid, even though the electron density can be small compared to the positive ion density, since the electron mobility is much higher than the ion mobility. Still if $F \ll 1$, the negative ion flux, Eq. (5b), is very small compared with the positive ion flux ($F/2$ times smaller), and the electron flux is practically equal to the positive ion flux. In an ion-ion plasma, where electrons are nearly absent and $F \gg 1$, the electric field disintegrates, and ions and electrons diffuse freely. Note that ion-ion diffusion is automatically ambipolar for $\mu_p = \mu_n$.[1] Below we examine the evolution of species densities and fluxes under different scenarios of plasma losses, all under the condition of equal electron and ion temperatures.

As long as $F \ll 1$, the negative ion flux to the wall is very small. Therefore, the negative ion density is practically constant, while electrons are still present. The evolution of electron density can be found analytically. Since $n(x,t) = n(x,t=0) = n(0) = \mathrm{const}$, the continuity equation $\partial n_e/\partial t = Z_{e,\mathrm{loss}} n_e$ can be readily integrated using $Z_{e,\mathrm{loss}}$ of Table I.

$$\frac{\mu_i}{\mu_e}\ln\left(\frac{n_e(0)}{n_e(t)}\right) + \frac{1}{2}\ln\left(\frac{n_e(0)+n(0)}{n_e(t)+n(0)}\right) = t/\tau_d, \tag{7}$$

where $\tau_d \equiv \Lambda^2/D_i$. Equation (7) describes two different regimes in the afterglow, before and after a critical time t_{cr},

$$t_{\mathrm{cr}} = \frac{\tau_d}{2}\ln\left(\frac{p_0}{n_0}\right). \tag{8}$$

For $t < t_{\mathrm{cr}}$, the second term on the left-hand side (lhs) of Eq. (7) dominates and the solution is simply $n_e(t) + n(0) = [n_e(0) + n(0)]\exp(-2t/\tau_d)$, corresponding to ambipolar decay of positive ions. For $t > t_{\mathrm{cr}}$, the first term on the lhs of Eq. (7) becomes important, and Eq. (7) describes free electron diffusion, with $n_e \sim \exp(-D_e t/\Lambda^2)$. Note that all electrons have practically escaped within a finite time period t_{cr}, as observed in [18] and discussed in [19]. The finite time needed for practically all electrons to escape is a consequence of the sharp increase of the electron loss frequency Eq. (6c), as the electron density keeps decreasing. After all

[1] In the general case of unequal ion mobilities the electric field, $E = [(D_p - D_n)/(\mu_p p + \mu_n n)](\partial p/\partial x)$, yields an ion ambipolar diffusion coefficient equal to $2\mu_p\mu_n T_i/(\mu_p + \mu_n)$.

electrons have practically escaped, negative ions start to come out by free diffusion, and $n \sim \exp[-(t-t_{cr})/\tau_d]$ for $t > t_{cr}$.

These analytical results have been validated with numerical simulations using the system of Eqs. (3). Time was normalized with the diffusion time τ_d and mobilities were taken as $\mu_p = \mu_n$ and $\mu_e = 100\mu_n$. The initial profiles (at $t=0$) were taken according to the fundamental diffusion mode Eq. (4), and plasma chemical processes were neglected. Numerical simulation verified that the cos-like species density profiles remained unchanged during the temporal evolution in the afterglow. The central species densities vs dimensionless time are depicted in Fig. 1(a). It is seen that the electron density decays much faster than the ion density, whereas the negative ion density is initially constant. The frequency of electron diffusive loss $Z_{e,\mathrm{loss}}$ is shown in Fig. 1(b). At times greater than t_{cr}, where $t_{cr} = 0.5 \ln 2$ for the chosen conditions, the electron density is small ($F > 1$), and electrons diffuse freely, therefore $Z_{e,\mathrm{loss}}$ increases sharply. The agreement between analytical predictions and numerical simulation is quite good [Figs. 1(a) and 1(b)].

One can also see a good agreement [Fig. 1(c)] between the numerical results and analytical formulas [Eq. (5)] for fluxes. The transition from an electron-dominated plasma to an ion-ion (electronless) plasma occurs at time t_{cr}. At this time the negative ion flux increases abruptly and negative ions come out of the plasma. Therefore, we can also define t_{cr} as the time when negative ions first come out. The critical time decreases considerably with increasing electronegativity [20],

$$2t_{cr}/\tau_d \approx n_e/n \to 0 \quad \text{as} \quad n_e/n \to 0,$$

see Eq. (8). In an electron-dominated plasma, the positive ion flux evolves by ambipolar diffusion (with coefficient $2D_i$). In an ion-ion plasma, the positive ion flux evolves by free diffusion (with coefficient D_i). Therefore at the moment of transition from electron-dominated plasma to ion-ion plasma an abrupt drop (by two times) in the positive ion flux occurs [Fig. 1(c)].

Figure 2 depicts the establishment of the fundamental mode (cos-like profiles) starting from a steady-state plasma. The initial ($t=0$) species density profiles [Fig. 2(a)] correspond to the steady state of Eqs. (3) assuming small detachment and attachment compared with diffusion, i.e., $\nu_{\mathrm{att}}\tau_d = \gamma\tau_d = 0.1$, and no ion-ion recombination. We again assumed that, in the afterglow, the electron temperature drops rapidly to $T_e = T_i$. At steady state, negative ions pile up at the discharge center by the electrostatic field [Fig. 2(a)]. After a short time ($t/\tau_d = 0.4$) cos-like profiles [Fig. 2(c)] are formed and the analytic solutions for Eqs. (5)–(8) can be applied.

It is also interesting to look at the speed of propagation of negative ions towards the wall. The fluid velocity of negative ions is the ratio of negative ion flux to their density $V_n \equiv \Gamma_n/n$. In the plasma core, negative ions evolve by almost free diffusion, and the ion velocity is a linear function of space [see Figs. 2(a), 2(b), and 2(c)]. A little further out, where electronegativity is close to unity, the drift is compa-

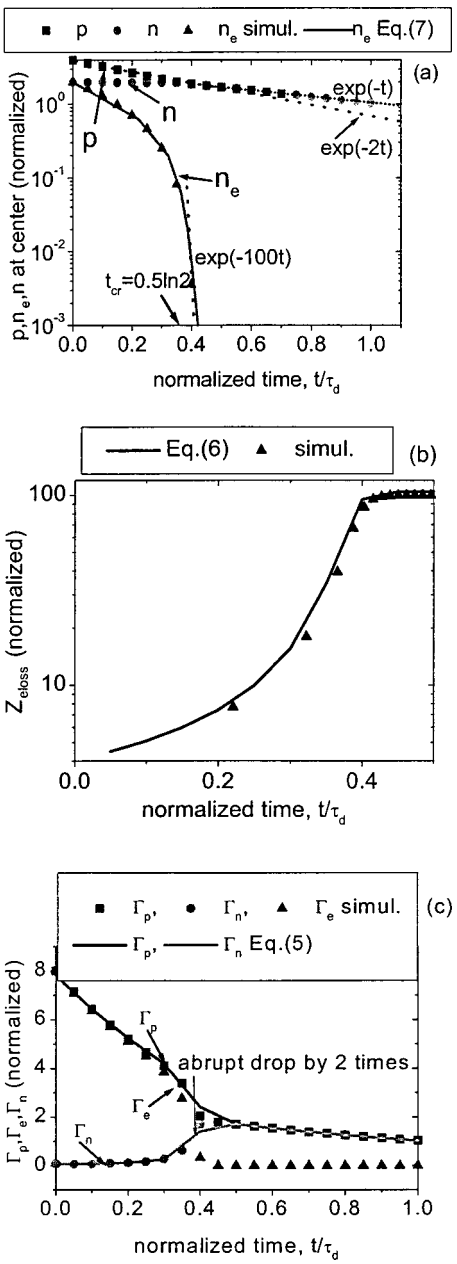

FIG. 1. Comparison of the results of numerical simulation of plasma decay in the afterglow with analytic estimates. The system of Eqs. (3) was solved numerically for the case when the electron and ion temperatures are equal $T_e = T_i$. Time was normalized with the ion diffusion time $\tau_d \equiv \Lambda^2/D_1$. Mobilities were taken as $\mu_p = \mu_n$ and $\mu_e = 100\mu_n$. The initial profiles (at $t=0$) were taken according to the fundamental diffusion mode Eq. (4), and plasma chemical processes were neglected in the afterglow. Plasma parameters vs dimensionless time: solid lines are analytical estimates, symbols are numerical results: (a) Densities of charged species at the centerline (normalized). The analytical solutions in an electron-dominated plasma [$p \sim \exp(-2t)$, $n \sim$ const], and in an ion-ion plasma [p, $n \sim \exp(-t)$] are also shown as limiting cases. (b) Electron diffusive loss frequency. Analytic estimate, Eq. (6), is shown as solid line. (c) Ion and electron fluxes (normalized) at the wall. Analytic estimates (solid lines) are according to Eq. (5).

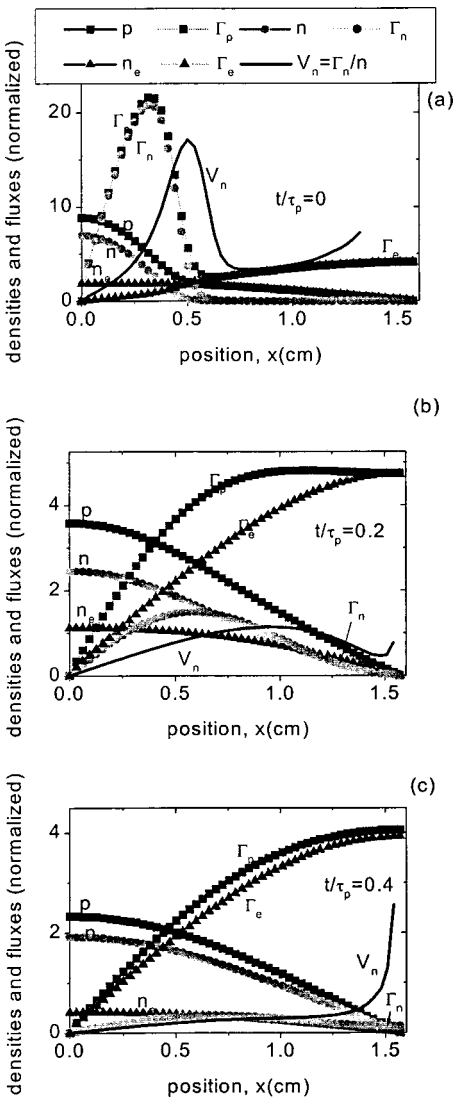

FIG. 2. Establishment of the fundamental diffusion mode (cos-like profiles) starting from steady-state plasma profiles. Plasma parameters are the same as in Fig. 1, but initial profiles correspond to the steady state of Eq. (3) with $T_e = T_i$ and small detachment and attachment compared with diffusion, $\nu_{\rm att}\tau_d = \gamma_d\tau_d = 0.1$. Also, no ion-ion recombination was taken into account. cos-like profiles are established after a dimensionless time of ~ 0.4.

rable with diffusion, so that the negative ion velocity diminishes. The negative ion density becomes exceedingly small near the wall, and the negative ion velocity starts increasing again. As the initially flat profile of electron density approaches a cos-like shape, the electric field increases in the core of the plasma, drift compensates diffusion, and the ion velocity drops [compare Fig. 2(b) with Fig. 2(c)].

IV. COMPARISON OF ANALYTICAL RESULTS WITH EXPERIMENTAL DATA

We now compare theoretical results with experimental data taken in the afterglow of a krypton-oxygen $Kr:O_2$, 1:1 gas mixture [21]. In this experiment, the discharge chamber

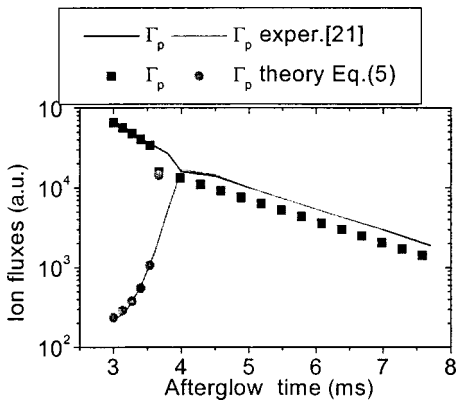

FIG. 3. Comparison of wall fluxes of positive and negative ions: lines are experimental data from [21], symbols are theoretical predictions according to Eq. (5).

was a cylinder of radius $R = 5.5$ cm and length $L = 18$ cm. Since $L \gg R$ the main plasma losses are across the radius, and a one-dimensional description is applicable. According to the value of the measured plasma potential, the electron temperature is close to the gas temperature at times in the afterglow $t > 0.5$ ms. The negative ion flux is very small for $t < 3.0$ ms, and increases abruptly after $t = 3.0$ ms (see Fig. 3). Dissociative attachment of electrons to oxygen molecules is not possible in an afterglow with cold electrons, since attachment requires electrons with energy of at least 0.6 eV [19]. The detachment rate depends on the densities of oxygen atoms and excited oxygen molecules, which were not measured. According to the experimental data (see Fig. 3), at the late stages of the afterglow, the negative and positive ion fluxes coincide, which implies that under these conditions detachment is small and can be neglected (see Sec. VII below for more details).

After a short initial period, all charged species density profiles should become similar and proportional to a zero-order Bessel function $\sim J_0(2.4r/R)$. The temporal evolution of fluxes is described by Eqs. (5) and the densities are found using the diffusive loss frequencies, Eqs. (6), written in cylindrical coordinates. The fluxes are presented in Fig. 3 jointly with the experimental data of [21]. The ratio of electron to ion mobility was taken as $\mu_e/\mu_i = 167$ [22]. As can be seen in Fig. 3, the slope of decay of the positive ion flux in an electron-dominated plasma ($t < 4$ ms) is approximately twice the slope in an ion-ion plasma ($t > 4$ ms) in agreement with the theory described in the previous section [Fig. 1(c)].

For comparison with the data, the ion densities $[p(t_0), n(t_0)]$ should be known at some moment of time t_0. Since the fluxes were reported only after 3 ms into the afterglow, we have chosen time $t_0 = 3$ ms as the reference time for calculation. The experimental data for the negative ion density are not reliable. Thus, we estimate the ratio of negative to positive ion densities (at $t_0 = 3$ ms) using the given experimental values for fluxes. At the critical time $t_{\rm cr} = 4$ ms, the positive and negative ion fluxes are equal, which indicates that electrons have disappeared by that time. The negative ion density is constant (no negative ion losses) and

smaller than the positive ion density for $t<t_{cr}=4$ ms, while for $t>t_{cr}=4$ ms the positive and negative ion densities are equal (ion-ion plasma). Thus, $n(t_0)=p(t_{cr})$, where $p(t_{cr})$ is the positive ion density at time t_{cr}. Now, the positive ion density is proportional to the ion flux, so that

$$\frac{p(t_{cr})}{p(t_0)}=\frac{\Gamma_p(R,t_{cr}-0)}{\Gamma_p(R,t_0)},$$

where $t_{cr}-0$ denotes that the flux should be evaluated just before the transition from electron-dominated to ion-ion plasma. Substitution of experimental flux values gives $n(t_0)/p(t_0)=0.48$. This ratio of densities is close[2] to the experimental measurement of densities shown in Fig. 10 of [21]. Knowing the ratio of ion densities we can estimate the critical time using Eq. (8). The value of τ_d can be deduced from the slope of the positive ion flux decay (Fig. 3) as $\tau_d=0.85$ ms. Thus, $t_{cr}=3+0.85\ln(1/0.48)=3.63$ ms. This estimate is a bit smaller than the experimental value of 4 ms. The difference between the two may be due to the influence of detachment as discussed below.[3]

V. AFTERGLOW WITH EQUAL ION AND ELECTRON TEMPERATURES ($T_i=T_e$) WITH ACCOUNT OF DIFFUSIVE LOSSES, ATTACHMENT, AND DETACHMENT

We assume that ion-ion recombination is slow compared with attachment and can be neglected during the first stage of the afterglow.[4] In general, attachment and detachment can vary considerably in the afterglow compared with the steady-state discharge. In less electronegative gases (e.g., oxygen), electron dissociative attachment has a relatively high-energy threshold, and the attachment rate is small in the afterglow. In highly electronegative gases, (e.g., chlorine), the attachment rate can increase considerably in the afterglow [23]. Associative detachment in the afterglow can occur via reactions of atoms with metastable molecules, and can generate fast electrons [19]. If the attachment frequency is small $\nu_{att}t_{cr}\ll 1$ electron decay is determined entirely by diffusive losses, and the theory of Sec. III applies. The opposite case is less straightforward. Indeed, if the attachment frequency is much larger than the initial diffusive loss frequency of electrons $[Z_{e,loss}\approx 2p_0/(\tau_d n_{e0})]$, the attachment losses dominate initially. However, as the electron density decreases, $Z_{e,loss}$ increases [Fig. 1(b)], and the diffusive loss to the wall starts to dominate attachment. Thus, even in this case we can expect the same phenomenon of electron disappearance within a finite time. To find the electron density temporal evolution and the critical time, we need to solve the electron continuity Eq. (3b). Since both attachment and detachment rates are linear functions of charged species densities, the spatial profiles again tend to the fundamental mode, see Eq. (4). Thus, the previous results for diffusive loss frequencies [Eqs. (6)], are valid in this case too. As we have seen, in a plasma with electrons, the negative ion diffusive loss is nearly zero. Therefore, the time rate of change of the electron density is equal to that of the positive ion density minus the rate of attachment plus the rate of negative ion detachment,

$$\frac{\partial n_e}{\partial t}=\frac{\partial p}{\partial t}-\nu_{att}n_e+\gamma_d(p-n_e). \tag{10}$$

The positive ion loss frequency [Eq. (6a)] is constant, and $p(t)=p_0\exp(-2t/\tau_d)$. The solution to Eq. (10) is now readily derived,

$$n_e(t)=\lambda p_0 e^{-2t/\tau_d}+(n_{e0}-\lambda p_0)\exp[-(\nu_{att}+\gamma_d)t], \tag{11}$$

where $\tilde{\nu}_{att}=\nu_{att}\tau_d/2$, $\tilde{\gamma}_d=\gamma_d\tau_d/2$, and $\lambda=(1-\tilde{\gamma}_d)/(1-\tilde{\nu}_{att}-\tilde{\gamma}_d)$.

VI. ANALYTICAL SOLUTIONS WITH ACCOUNT OF DIFFUSIVE LOSSES AND ATTACHMENT ONLY

We now focus on the influence of attachment assuming that the detachment frequency is zero ($\gamma_d=0$) in the afterglow. For short times, $\nu_{att}t_{cr}\ll 1$, Eq. (11) collapses to the previous result, Eq. (8). For longer times, $\nu_{att}t_{cr}\gg 1$, the electron density reduces to zero within a finite time t_{cr}, found by setting $n_e=0$ in Eq. (11). Thus,

$$t_{cr}=\frac{\tau_d/2}{\tilde{\nu}_{att}-1}\ln\left(\frac{n_0+\tilde{\nu}_{att}n_{e0}}{n_0+n_{e0}}\right), \tag{12a}$$

as found in [17]. An experimental diagnostic for measuring the attachment frequency was developed in [18] based on Eq. (12a). Now, when $\nu_{att}\tau_d\ln(p_0/n_0)\gg 1$, i.e., when attachment dominates diffusion loses initially, the critical time reduces to

$$t_{cr}=\frac{1}{\nu_{att}}\ln\left(\frac{\nu_{att}\tau_d n_{e0}}{2p_0}\right). \tag{12b}$$

Although attachment may dominate diffusion losses initially, diffusion will eventually take over since the frequency of electron diffusive loss increases with time.

In Fig. 4, the critical time for electron disappearance $t_{cr}=t_{n,out}$ is depicted as a function of the attachment frequency, for various ratios of initial negative ion to electron density (electronegativity). One can see that at small attachment frequencies $\tilde{\nu}_{att}\ll 1$, the critical time is close to that predicted by Eq. (8) where only diffusive losses are taken into account. In this case, the critical time depends crucially on the electronegativity. In the opposite case, ($\tilde{\nu}_{att}\gg 1$), the critical time is a few ν_{att}^{-1} and depends only weakly on electronegativity.

[2]Unfortunately, direct comparison is not possible since the experimental data for densities and ion fluxes in [21] have different time scales.

[3]Another possible explanation is that the experimental setup of [21] could not follow sharp increases of the negative ion flux.

[4]Generalization can be easily made by adding additional ion losses. We omit recombination in order not to overcomplicate the problem.

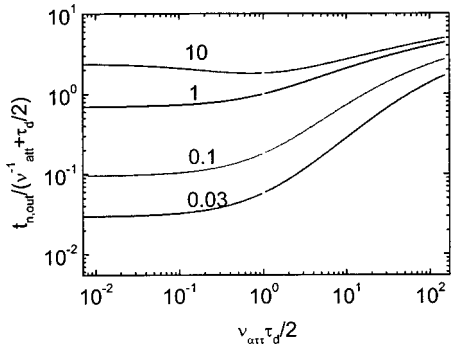

FIG. 4. Critical time to transition from an electron-dominated plasma to an ion-ion plasma as a function of attachment frequency, at various (initial) negative ion to electron density ratios. Detachment and ion-ion recombination are neglected.

VII. ANALYTICAL SOLUTIONS WITH ACCOUNT OF DIFFUSIVE LOSSES AND DETACHMENT. THEORY OF SELF-TRAPPING OF NEGATIVE IONS DUE TO DETACHMENT

In this section we shall focus on the role of negative ion detachment on the spatiotemporal dynamics of charged species in the afterglow [29]. In Fig. 5, results of numerical calculations of the central densities and wall fluxes are depicted for various attachment and detachment frequencies. Importantly, the value of the negative ion flux flowing to the wall greatly depends on the value of detachment frequency [compare Figs. 5(a) and 5(b)].

Indeed, if the detachment frequency is larger than the diffusive loss frequency, negative ions convert to electrons during their diffusion towards the wall. As a result, a substantial number of electrons remain even in the late afterglow. The presence of these electrons results in ''self-trapping'' of negative ions, due to emerging electric field. As we shall see, the critical value of detachment frequency is given by $\gamma_d\tau_d=2$. If $\gamma_d\tau_d>2$, the wall flux of negative ions is very small even in the late afterglow [Fig. 5(b)].

Let us now find an analytic solution valid for the late afterglow, when all charged species spatial profiles are similar. In this case, the species continuity equations simplify to

$$\frac{\partial n}{\partial t}=-\tau_d^{-1}n\frac{F}{F+1}+\nu_{\rm att}n_e-\gamma_d n \tag{13a}$$

for negative ions, and

$$\frac{\partial p}{\partial t}=-\tau_d^{-1}p\left(1+\frac{1}{1+F}\right), \tag{13b}$$

for positive ions. Parameter $F\equiv\mu_i(p+n)/(\mu_e n_e)$ is the same as before, Eq. (5).

In the late afterglow, electrons and ions decay with the same decay frequency (see parallel slopes in Fig. 5),

$$\frac{\partial n}{n\,\partial t}=\frac{\partial n_e}{n_e\partial t}=\frac{\partial p}{p\,\partial t}\equiv\nu_{\rm decay}.$$

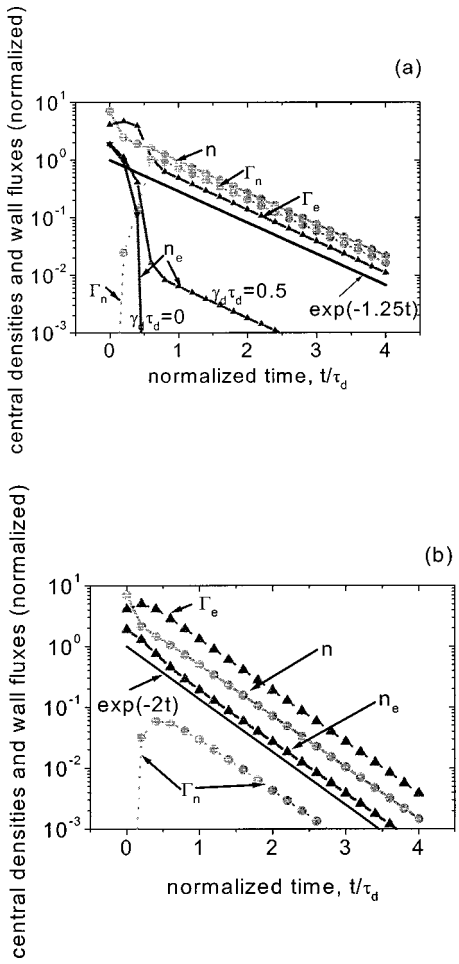

FIG. 5. The temporal evolution of central charged species densities and wall fluxes as functions of dimensionless time (normalized by τ_d). Plasma parameters are the same as in Fig. 1, but with detachment and attachment in the afterglow taken into account. (a) $\nu_{\rm att}\tau_d=\gamma_d\tau_d=0.5$. For comparison, the electron density evolution for $\nu_{\rm att}\tau_d=\gamma_d\tau_d=0$ is also shown. (b) $\nu_{\rm att}\tau_d=\gamma_d\tau_d=3$.

Equations (13) can now be combined to obtain a quadratic equation for y, the ratio of electron to negative ion density (inverse electronegativity) $y\equiv n_e/n$,

$$\frac{F(y)}{F(y)+1}+(\tilde\gamma_d-1)=\tilde\nu_{\rm att}y, \tag{14}$$

where F has been rewritten as an explicit function of y, i.e., $F(y)\equiv(\mu_i/\mu_e)(y+2)/y$.

Equation (14) has two roots, one of which is negative and thus nonphysical. If $\tilde\gamma_d<1$, the right-hand side of Eq. (14) can be neglected (assuming $\mu_i\tilde\nu_{\rm att}/\mu_e\ll1$). One obtains $F+1=1/\tilde\gamma_d$ and $y=(\mu_i/\mu_e)[2\tilde\gamma_d/(1-\tilde\gamma_d)]$, i.e., a very small electron density (since $\mu_i/\mu_e\ll1$ and $\tilde\gamma_d<1$). Substituting F into Eq. (5) one finds the corresponding ratios of wall fluxes,

$$\frac{\Gamma_e}{\Gamma_p}=\frac{2\overline{\gamma}_d}{1+\tilde\gamma_d}\quad\text{and}\quad\frac{\Gamma_n}{\Gamma_p}=\frac{1-\tilde\gamma_d}{1+\tilde\gamma_d}. \tag{15}$$

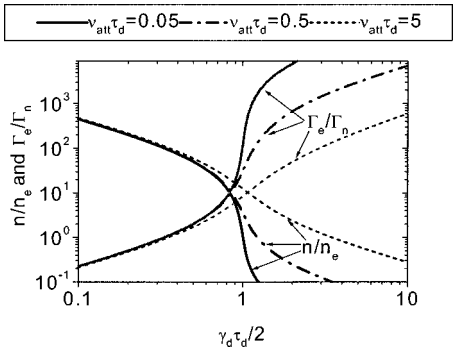

FIG. 6. The negative ion to electron density ratio [solution of Eq. (14)] and the electron to negative ion flux ratio are shown as a function of detachment frequency for different attachment frequencies in the late afterglow.

Physically, this means that electrons are quickly removed by free diffusion. The diffusive loss frequency of positive ions [Eq. 6(a)] turns out to be $Z_{p,\mathrm{loss}}=\nu_{\mathrm{decay}}=1+\tilde{\gamma}_d$. For small $\tilde{\gamma}_d$, the charged species fluxes in the late afterglow correspond to free electron and ion diffusion. When $\tilde{\gamma}_d\to 1$, the electron density does not decay as quickly and the electric field accelerates positive ions to make their diffusive loss frequency equal to $Z_{p,\mathrm{loss}}=2$; the limit for electron-dominated plasma. Numerical calculations [Fig. 5(a)], give a value of $Z_{p,\mathrm{loss}}=1.25$ for $\tilde{\gamma}_d=0.25$ that coincides with the analytical estimate. For $\tilde{\gamma}_d<1$, the electron flux in the late afterglow is produced by detachment of negative ions during their free diffusion. This implies that the electron flux is proportional to $\gamma_d\tau_d$. Numerical calculation gives $\Gamma_n/\Gamma_e=1.5$ for $\tilde{\gamma}_d=0.25$ that coincides with the analytical estimate.

On the other hand, if $\tilde{\gamma}_d>1$, the physical picture changes drastically. The solution to Eq. (14) yields for electronegativity and the flux ratios

$$y=\frac{\tilde{\gamma}_d-1}{\tilde{\nu}_{\mathrm{att}}},\quad \frac{\Gamma_e}{\Gamma_p}=1,\quad \text{and}\quad \frac{\Gamma_n}{\Gamma_p}=\frac{\mu_i}{\mu_e}\frac{y+2}{y(1+y)}. \quad (16)$$

This corresponds to a relatively large number of electrons in the afterglow. The presence of these electrons causes negative ions to be trapped. Positive ions diffuse with ambipolar diffusion to the wall and their density decays with a time constant of $\tau_d/2$, approximately twice as fast compared to the case $\tilde{\gamma}_d<1$, as can also be seen in Fig. 5. The analytical result, Eq. (16), coincides with the numerical calculation. For example, the analytical estimate by Eq. (16) is $y=0.33$ for $\tilde{\gamma}_d=\tilde{\nu}_{\mathrm{att}}=1.5$, which agrees closely with the numerical result of $y=0.34$.

In Fig. 6, the solution to Eq. (14) and the electron to negative ion flux ratio in the late afterglow are shown as a function of detachment frequency for different attachment frequencies. For $\tilde{\gamma}_d<1$, the flux ratio does not depend on the attachment frequency (attachment is still slow compared to free electron diffusion), and is determined only by the detachment frequency. For this case, the electron density is small (n/n_e is large) since electrons escape with nearly free diffusion. In the opposite case, $\tilde{\gamma}_d>1$, the negative ion flux to the wall is nearly zero. Negative ions trap themselves by producing electrons through detachment on ''their way'' to the walls. In the limit $\mu_i/\mu_e\to 0$, Eq. (14) describes a transcritical bifurcation at $\gamma_d\tau_d=2$ [Ref. [24]].

Thus, we can draw an important conclusion that negative ions can be extracted in the afterglow only if $\gamma_d\tau_d<2$. This implies that negative ion sources should operate at low pressures and not too large gaps, since $\gamma_d\tau_d=\gamma_d\Lambda^2/D_i \sim \gamma_d PL^2$.

VIII. AFTERGLOW WITH $T_i \ll T_e$

A relatively high electron temperature in the afterglow may be sustained because of: (a) electron-metastable superelastic collisions, (b) electron detachment in the afterglow, and/or (c) a small residual power in the afterglow. In practical systems this may result by a capacitively coupled rf bias applied during the afterglow; see, for example, [25,26]. Capacitive coupling in the afterglow may be an efficient mechanism of electron heating. Solving the electron energy equation we found that a residual power in the afterglow as small as 1% of the power during the active glow can keep electrons warm with $T_e\sim 1$ eV.

What is the effect of a relatively large electron temperature ($T_e\gg T_i$) on the possibility of negative ion extraction out of the plasma? To analyze this situation we again assume, for simplicity, a fixed electron temperature in the afterglow. We also assume that attachment, detachment, and ion-ion recombination can be neglected in the afterglow compared to drift and diffusion. At the expense of generality due to these simplifications we are able to find analytical estimates for the time required for negative ions to start leaving the discharge, and to explore the underlying physics.

If $T_i\ll T_e$, negative ions are piled up at the discharge center when the attachment frequency is small compared to the diffusion time (see exact criterion in [7,14,27]). In Fig. 7 one can see the time evolution of species density profiles for $T_i/T_e=0.01$. These results were obtained by numerical solution of Eqs. (3). Initially, negative ions are absent at the plasma edge ($x>0.5$); an electron-ion plasma exists in this region. The presence of an electron-ion plasma region changes considerably the temporal evolution in comparison with the case of $T_i=T_e$. When $T_i=T_e$, the density profiles become similar after some initial evolution. After that time all profiles evolve simultaneously. Negative ions are present everywhere practically at all times, and the effective electron diffusion coefficient [Eq. (3e)] is substantially uniform.

In the present case ($T_i\ll T_e$), the ratio n/n_e is very large at the discharge center (ion-ion core) and approaches zero near the edge. Therefore, D_{eff} is very inhomogeneous, large in the ion-ion core $D_{\mathrm{eff}}\approx\mu_i T_e(p+n)/n_e$, and small in the edge region $D_{\mathrm{eff}}\approx\mu_i T_e$. The frequency of electron loss $Z_{e,\mathrm{loss}}$, which is determined by the slow diffusion in the edge region, is changing relatively slowly at first. Normalizing time by $\tau_d=\Lambda^2/(\mu_i T_e)$, the normalized frequency of electron loss is close to *unity* until the electron-ion plasma region vanishes. From Fig. 8(c) one can see that, notwithstanding the fact that the ratio n/n_e is very large at the plasma center (the effective diffusion coefficient is also very large there), the frequency of electron loss is still close to *unity*

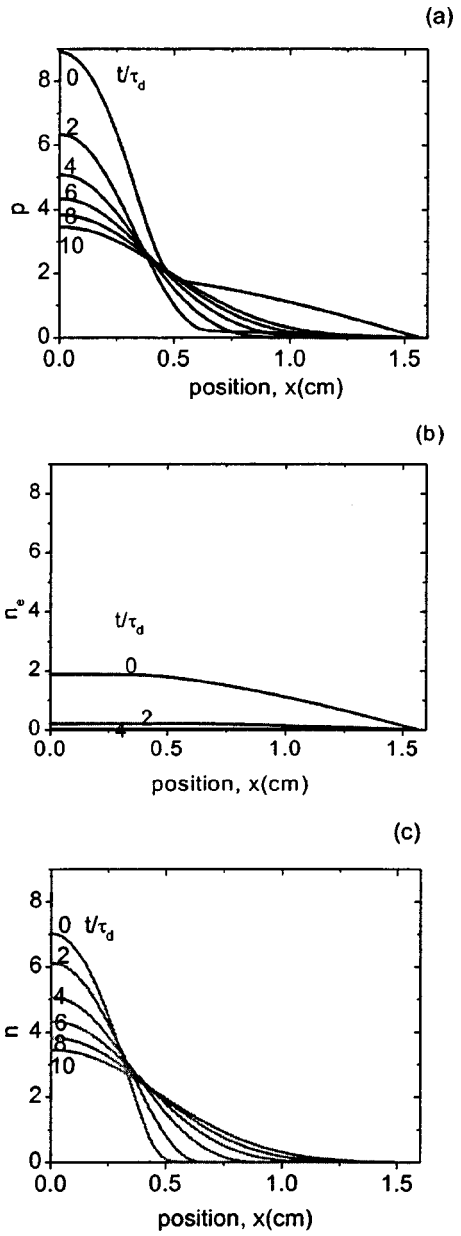

FIG. 7. Spatiotemporal evolution of charged species densities [time is normalized by $\tau_d \equiv (T_i/T_e)(\Lambda^2/D_i)$]. Plasma parameters are the same as in Fig. 1, but $T_e = 100T_i$. (a) positive ions, (b) electrons, and (c) negative ions.

(for times<5). Note the difference with the case $T_e = T_i$ in Fig. 1(b).

One can show analytically that even though the plasma profiles change with time, $Z_{e,\mathrm{loss}}$ varies slowly, as long as an electron-ion plasma edge remains in the discharge vessel. Let us assume that in the presence of negative ions ($0 < x < L_{\mathrm{ii}}$) the effective electron diffusion coefficient is infinitely large, and in the region where negative ions are absent ($L_{\mathrm{ii}} < x < L$), the effective diffusion coefficient is equal to the ambipolar diffusivity $D_{\mathrm{eff}} = D_{\mathrm{amb}} \approx \mu_i T_e$. Here L_{ii} is half of the extent of the ion-ion core and L is half of the interelectrode gap (the sheath has been assumed very thin). Because of the large diffusivity in the ion-ion core, the electron density profile is flat. In the edge region of electron-ion plasma ($L_{\mathrm{ii}} < x < L$), the electron density is described by a linear diffusion equation,

$$\frac{\partial n_e}{\partial t} = D_{\mathrm{amb}} \frac{\partial^2 n_e}{\partial x^2}.$$

The boundary condition at $x = L_{\mathrm{ii}}(t)$ is

$$D_{\mathrm{amb}} \frac{\partial n_e}{\partial x} = \frac{\partial n_e}{\partial t} L_{\mathrm{ii}}(t)$$

which is a consequence of continuity. The diffusion equation is separable and has an analytic solution,

$$n_e(x,t) = n_e(0,0) \frac{\sin[\kappa(L-x)]}{\sin[\kappa(L-L_{\mathrm{ii}})]} e^{-Z_{e,\mathrm{loss}} t}, \quad \text{where}$$

$$Z_{e,\mathrm{loss}} = D_{\mathrm{amb}} \kappa^2 \quad \text{and} \quad \kappa L_{\mathrm{ii}} \tan[\kappa(L-L_{\mathrm{ii}})] = 1. \quad (17)$$

In Fig. 8(d), the analytic solution for dimensionless $Z_{e,\mathrm{loss}}$, Eq. (17), is depicted as a function of L_{ii}/L. For example, for $L_{\mathrm{ii}} = 0.5L$ one obtains $\kappa L = 1.722$. The dimensionless electron loss frequency is then equal to 1.20. In the case of a spatially uniform ambipolar diffusion coefficient ($L_{\mathrm{ii}} = 0$ or $\kappa L = \pi/2$), $Z_{e,\mathrm{loss}} = 1$. Therefore, the approximation of infinitely large diffusion coefficient in the ion-ion core (flat electron density profile) results in an enhancement of electron loss by 20%. For $L_{\mathrm{ii}} = 0.7L$, the dimensionless electron loss frequency is only 1.7, a 70% enhancement. The growth of L_{ii}/L (expansion of the negative ion core) explains the increase of $Z_{e,\mathrm{loss}}$. Eventually, as $L_{\mathrm{ii}} \to L, Z_{e,\mathrm{loss}} \to D_{\mathrm{amb}}/[L/(L-L_{\mathrm{ii}})]$ becomes very large. The analytical results depicted in Fig. 8(d) were calculated using Eq. (17), where $L_{\mathrm{ii}}(t)$ was taken from numerical simulation as the point where $n_e(x,t) = n(x,t)$ (Fig. 7).

The negative ion motion is governed by the competition of diffusion and drift, see Eq. (3a). Negative ions diffuse almost freely in the ion-ion core, where $n_e \ll n$, i.e., drift is small compared to diffusion, since the electric field is correspondingly small. In the core, the positive and negative ion fluxes coincide, and the electron flux is much smaller than both of them $\Gamma_n \approx \Gamma_p \gg \Gamma_e$ (see Fig. 9). A comparison of the actual negative ion motion to free diffusive motion (not shown) revealed that, indeed, the evolution of negative ion density profiles approaches the free diffusion limit. In fact, the actual spatial profiles were found to coincide with the free diffusion profiles in the central region of the discharge. However, as expected, the actual negative ion density near the edge dropped more rapidly compared to the free diffusion profiles.

As the negative ion density decreases towards the edge, the electric field increases, reducing the negative ion flux to practically zero (Fig. 9). At that point, negative ions are almost in Boltzmann equilibrium,

$$T_i \frac{\partial n}{\partial x} \approx T_e \frac{n}{n_e} \frac{\partial n_e}{\partial x}.$$

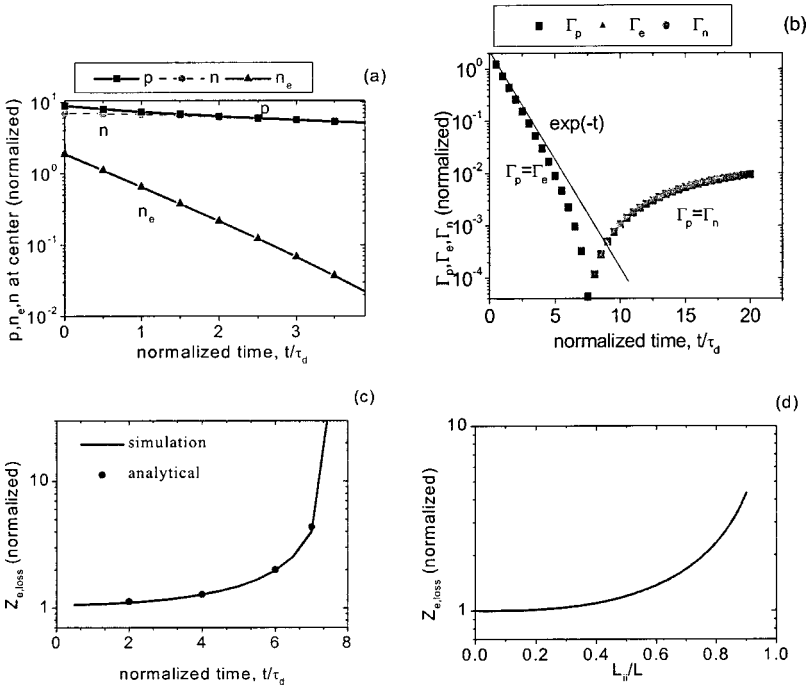

FIG. 8. Temporal evolution of plasma parameters as a function of dimensionless time [normalized by $\tau_d \equiv (T_i/T_e)(\Lambda^2/D_i)$]. Plasma parameters are the same as in Fig. 7. (a) Central densities. (b) Wall fluxes. (c) Frequency of diffusive electron loss as a function of time: numerical simulation (line) and analytical results (points). (d) Frequency of diffusive electron loss as a function of the ion-ion plasma core length according to Eq. (17).

This implies that the negative ion density drops nearly exponentially,

$$n \sim \exp(-x/\delta), \quad \text{where} \quad \delta = \frac{T_i}{T_e}\left(\frac{\partial \ln(n_e)}{\partial x}\right)^{-1},$$

forming a negative ion front. The front can be seen clearly in Fig. 9. The location of the front (the point where the negative ion density starts dropping rapidly) can be estimated from the condition of equality of electron and ion fluxes $\Gamma_n = \Gamma_e = \Gamma_P/2$. Based on this definition, the negative ion front velocity was found to be given by [8]

$$V_{\text{if}} = 2\sqrt{D_i Z_{e,\text{loss}}}. \tag{18}$$

Surprisingly, the negative ion front moves towards the wall with a nearly constant velocity V_{if} since $Z_{e,\text{loss}}$ is nearly constant, at least initially [Fig. 8(c) and 8(d)]. In Fig. 10 the points corresponding to $\Gamma_n = \Gamma_e$ (dashed line with dots) and $n_e = n$ (solid line) are shown, as found from numerical simulation. The analytic estimate (dotted line corresponding to $V_{\text{if}} = 2\sqrt{0.01 \times 1} = 0.2$) is very close to the calculated motion of negative ion front. When the negative ion front approaches the wall, $Z_{e,\text{loss}} \gg 1$ [time > 6, see Fig. 8(c)], and the front velocity increases. As it turns out, the points at which $n_e = n$ and $\Gamma_e = \Gamma_n$ move in a similar manner, so either equality can be used for defining the location of the negative ion front.

As we have seen, negative ions diffuse nearly freely in the core region ($n_e \ll n$) and slow down by the electric field in the edge region where $n_e > n$. It is interesting to find the maximum of the fluid velocity of negative ions $V_i \equiv \Gamma_n/n$. In the core region, the negative ion flux is a diffusion flux and

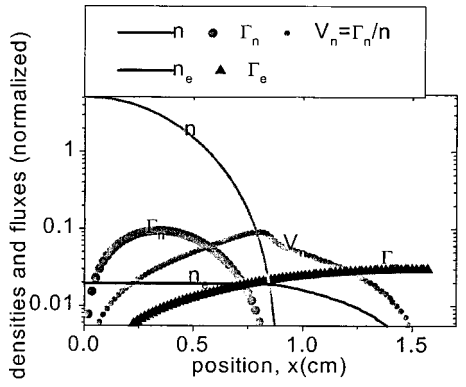

FIG. 9. Spatial profiles of negative ion and electron densities, and their fluxes at dimensionless time $t/\tau_d = 4$. Plasma parameters are the same as in Fig. 7. The negative ion fluid velocity V_n is also shown.

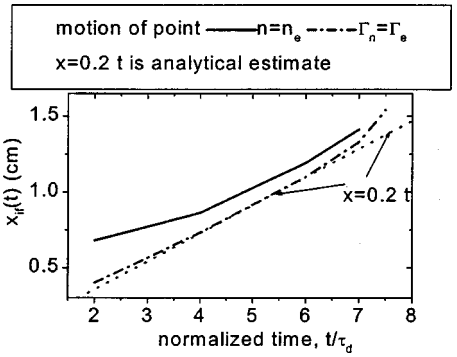

FIG. 10. Motion of negative ion front in the afterglow. Solid line corresponds to the motion of the point where the electron density is equal to the negative ion density as found from numerical simulation. Dashed line with dots corresponds to the motion of the point where the electron flux is equal to the negative ion flux as found from numerical simulation. Analytical estimate corresponding to constant front velocity is shown as dotted line.

$$V_i \equiv \frac{\Gamma_n}{n} = D_i \frac{\partial n}{n\,\partial x} = D_i \frac{x}{2D_i t} = \frac{x}{2t},$$

i.e., the negative ion fluid velocity is proportional to position and inversely proportional to time. The maximum velocity appears to be near $x_{\rm if}$, the location of the negative ion front found by setting $n_e(x_{\rm if},t)=n(x_{\rm if},t)$ (see Fig. 9), so $V_{i,\max}\approx x_{\rm if}/2t$. Thus, the maximum negative ion fluid velocity is smaller than the velocity of the negative ion front, the latter being $V_{\rm if}=dx_{\rm if}/dt\approx x_{\rm if}/t$. The velocity of the negative ion front is not equal to the velocity of negative ions at the position of the front. This phenomenon has an analogy in classical hydrodynamics, where the shock velocity $V_{\rm shock}=(\Gamma_+-\Gamma_-)/(n_+-n_-)$ is different than the fluid velocities to the right of the shock $V_{\rm shock}=\Gamma_+/n_+$ and to the left of the shock $V_{\rm shock}=\Gamma_-/n_-$ [28]. However, in classical hydrodynamic shocks, the value of the shock velocity lies in between the fluid velocities in front of and behind the shock. In contrast to the classical hydrodynamic shocks, the velocity of the negative ion front is faster than the velocity of the negative ion fluid on either side of the shock (or everywhere in the discharge for that matter). This is the consequence of the fact that electrons, which can move much faster than negative ions, influence the front motion.

Knowing the velocity of the negative ion front, one can find the time needed for negative ions to reach the wall, $t_{n,\rm out}$. This time is the sum of $t_{\rm ii}$, the time after which negative ions start to diffuse nearly freely, and the time needed for the front to reach the wall,

$$t_{n,\rm out}=t_{\rm ii}+\frac{L-L_{\rm ii0}}{V_{\rm if}}, \tag{19}$$

where again $L_{\rm ii0}$, can be determined by the attachment and detachment frequencies [7,14,27]. For the numerical example discussed above (Fig. 10),

$$t_{n,\rm out}=1.6+\frac{1.57-0.36}{0.2}=1.6+6.1=7.5,$$

which nearly coincides with the simulation result.

Further simulations were performed for a range of ratios of ion to electron temperatures and for different initial conditions. Table II(a) shows the numerically calculated time when negative ions appear at the wall compared to the analytic estimate, Eq. (19). The analytical estimate is quite accurate. As the ratio of ion to electron temperatures tends to unity, the edge region of electron-ion plasma (without negative ions) disappears and the concept of negative ion front fails. Then, the theory of Sec. III applies.

Table II(b) shows the time when negative ions appear at the wall calculated numerically and compared with the analytic estimate, Eq. (19), for different initial density of negative ions at steady-state (using various attachment frequencies and a constant detachment frequency), $T_i/T_e=0.01$, and fixed total electron density ($\int n_e dx=2$). This amounts to varying plasma electronegativity. Since the total amount of negative ions is conserved until negative ions come out (negative ion chemistry has been neglected compared to diffusion), we characterize different cases by the values of the integral $\int n\,dx$. Again, the analytical estimate, Eq. (19), predicts $t_{n,\rm out}$ reasonably well. For large $\int n\,dx$ the ion-ion core expands towards the wall and occupies almost the entire discharge space. In such case Eq. (19) is not valid, since it was derived under the assumption that the ion-ion core initially occupies a narrow region in the discharge center [8]. Determining the time negative ions first reach the wall is important for applications in negative ion sources and charge-free semiconductor manufacturing [11].

TABLE II. Time $t_{n,\rm out}$ when negative ions first come out [normalized by $\Lambda^2/(\mu_i T_e)$] (a) for various temperature ratios T_i/T_e and (b) for various electronegativities.

(a)

T_i/T_e	$t_{n,\rm out}$ simulation	$t_{n,\rm out}$ analytic
0.1	2.3	3.1
0.05	3.3	3.6
0.01	7.5	7.5
0.005	10.1	9.35

(b)

$\int n\,dx$	$L_{\rm ii}$	$t_{n,\rm out}$ simulation	$t_{n,\rm out}$ analytic
2	0.36	7.5	7.5
6	0.6	6.3	6.6
18	0.86	4.6	4.6
48	1.1	2.7	3.3

IX. CONCLUSIONS

The spatiotemporal evolution of charged species densities and wall fluxes during the afterglow of an electronegative discharge has been investigated. The decay of a plasma with negative ions consists of two stages. During the first stage of the afterglow, electrons dominate plasma diffusion and negative ions are trapped inside the vessel by the static electric field; the flux of negative ions to the walls is nearly zero. During this stage, the electron escape frequency increases considerably in the presence of negative ions, and can eventually approach free electron diffusion. During the second stage of the afterglow, electrons have disappeared, and positive and negative ions diffuse to the walls with the ion-ion ambipolar diffusion coefficient.

Analytic expressions for the time required for negative ions to reach the wall $t_{n,\rm out}$, were derived for two limiting cases of equal and very different electron and ion temperatures, in the afterglow of electronegative gas plasmas.

When $T_i=T_e$ and no volume plasma chemical reactions are taken into account, electrons disappear (and negative ions come out) in a finite time $t_{n,\rm out}=t_{\rm cr}=(\Lambda^2/2\mu_i T)\ln(p_0/n_0)$. This time considerably decreases with increasing electronegativity.

If attachment is important in the afterglow (strongly electronegative gases, such as Cl_2) the time of electron density

decay becomes shorter. However, even if the attachment frequency (ν_{att}) is initially larger than the electron diffusive loss frequency, diffusion eventually dominates during the late stages of the afterglow. In this case, the time required for electrons to disappear is also finite and is given by

$$t_{n,\mathrm{out}} = t_{\mathrm{cr}} = \frac{1}{\nu_{\mathrm{att}}} \ln\left(\frac{\nu_{\mathrm{att}} \tau_d n_{e0}}{2 p_0}\right).$$

If detachment is important in the afterglow (weakly electronegative gases, such as O_2) the time of electron density decay becomes longer. This case depends crucially on the product of detachment frequency and ion diffusion time $\gamma_d \tau_d$. If $\gamma_d \tau_d > 2$, negative ions convert to electrons during their diffusion towards the wall. As a result, a substantial number of electrons appear even in the late afterglow. The presence of these electrons results in ''self-trapping'' of negative ions, due to emerging electric field, and the negative ions flux at the walls is very small. In the opposite case, $\gamma_d \tau_d < 2$, the physical picture changes drastically: electrons eventually escape nearly freely, and the negative ion flux equals the positive ion flux. The transition between the two cases is abrupt and can be described mathematically as a transcritical bifurcation. Thus, negative ions can be extracted in the afterglow only if $\gamma_d \tau_d < 2$. This implies that negative ion sources should operate at low pressures and not too large gaps.

When $T_i \ll T_e$, negative ion density fronts may from during the afterglow. These fronts are not analogous to hydrodynamic shocks. Negative ions diffuse freely in the plasma core, but the negative ion front propagates towards the chamber walls with a nearly constant velocity $V_{\mathrm{if}} = \sqrt{4 D_i Z_{e,\mathrm{loss}}}$, (for constant electron and ion temperatures). The negative ion fronts are a new type of nonlinear structure, different from hydrodynamic nonlinear waves and beyond the classification of dissipative structures (see, e.g., [30]). The evolution of ion fronts in the afterglow of electronegative plasmas is important, since it determines the time needed for negative ions to reach the wall, and thus influences surface reactions in plasma processing.

ACKNOWLEDGMENTS

Fruitful discussions with Professor A. Lichtenberg, Professor L. Tsendin, and Professor R. Franklin are greatly acknowledged. This work was funded by the National Science Foundation (CTS-9713262 and CTS-0072854), and the State of Texas through the Texas Advanced Technology Program. I.K. was supported in part by the Princeton Plasma Physics Laboratory University Research Support Program.

[1] T. H. Ahn, K. Nakamura, and H. Sugai, Plasma Sources Sci. Technol. **5**, 139 (1996).
[2] G. S. Hwang and K. P. Giapis, Phys. Rev. Lett. **79**, 845 (1997).
[3] M. B. Hopkins and K. N. Mellon, Phys. Rev. Lett. **67**, 449 (1991).
[4] D. Hayashi and K. Kadota, J. Appl. Phys. **83**, 697 (1998).
[5] W. Swider, *Ionospheric Modeling* (Birkhauser Verlag, Basel, 1988).
[6] T. Takeuchi, S. Iizuka, and N. Sato, Phys. Rev. Lett. **80**, 77 (1998).
[7] I. D. Kaganovich, L. D. Tsendin, Plasma Phys. Rep. **19**, 645 (1993).
[8] I. D. Kaganovich, D. J. Economou, B. N. Ramamurthi, and V. Midha, Phys. Rev. Lett. **84**, 1918 (2000).
[9] Y. Watanabe, M. Shiratan, Y. Kubo, L. Ogawa, and S. Ogi, Appl. Phys. Lett. **53**, 1263 (1988).
[10] Charles, R. Boswell, and H. Kuwara, Appl. Phys. Lett. **67**, 40 (1995).
[11] V. Midha and D. J. Economou, Plasma Sources Sci. Technol. **9**, 256 (2000).
[12] A. Smith and L. J. Overzet, Plasma Sources Sci. Technol. **8**, 82 (1999).
[13] M. V. Malyshev, V. M. Donnelly, and S. Samukawa, J. Appl. Phys. **86**, 4813 (1999).
[14] L. D. Tsendin, Zh. Tekh. Fiz. **59**, 21 (1989) [Sov. Phys. Tech. Phys. **34**, 11 (1989)].
[15] A. V. Phelps, J. Res. Natl. Inst. Stand. Technol. **95**, 407 (1990).
[16] M. V. Koniukov, Zh. Eksp. Teor. Fiz. **34**, 908(1958) [Sov. Phys. JETP **12**, 629 (1958)].
[17] H. Massey, *Negative Ions*, 3rd ed. (Cambridge University Press, Cambridge, UK, 1976), p. 741.
[18] L. J. Puckett, M. D. Kregel, and M. W. Teague, Phys. Rev. A **4**, 1659 (1971).
[19] S. A. Gutsev, A. A. Kudryavtsev, and V. A. Romanenko, Tech. Phys. **40**, 1131 (1995).
[20] A. A. Kudryavtsev, Tech. Phys. Lett. **22**, 693 (1996).
[21] D. Smith, A. G. Dean, and N. S. Adams, J. Phys. D **7**, 1944 (1974).
[22] B. M. Smirnov, *Physics of Weakly Ionized Gases (Problems and Solutions)* (Mir, Moscow, 1981), p. 430.
[23] S. Ashida and M. A. Lieberman, Jpn. J. Appl. Phys., Part 1 **36**, 854 (1997).
[24] J. Guckenheimer and P. Holmes, in *Nonlinear Oscillations, Dynamical Systems, and Bifurcations of Vector Fields*, Applied Mathematical Sciences, Vol. 42 (Springer, New York, 1986).
[25] L. J. Overzet, Yun Lin, and L. Luo, J. Appl. Phys. **72**, 5579 (1992).
[26] H. Amemiya, in *Dusty and Dirty Plasmas, Noise, and Chaos in Space and in Laboratory*, edited by H. Kikuchi (Plenum, New York, 1994).
[27] J. Lichtenberg, I. G. Kouznetsov, T. D. Lee, M. A. Lieberman, I. D. Kaganovich, and L. D. Tsendin, Plasma Sources Sci. Technol. **6**, 437 (1997).
[28] G. B. Whitham, *Linear and Nonlinear Waves* (Wiley, New York, 1974).
[29] I. D. Kaganovich, B. N. Ramamurthi, and D. J. Economou, Appl. Phys. Lett. **76**, 2844 (2000).
[30] B. S. Kerner and V. V. Osipov, Usp. Fiz. Nauk. **160**, 1 (1990) [Sov. Phys. Usp. **33**, 679 (1990)].